Geophysical Research Letters

RESEARCH LETTER
10.1029/2025GL119421

Increasing Frequency and Persistence of the Summertime Greenland High Regime Not Captured by a Seasonal Prediction Model Very Large Ensemble

Simon H. Lee[1] **and Lorenzo M. Polvani**[2,3,4]

[1]School of Earth and Environmental Sciences, University of St Andrews, St Andrews, UK, [2]Department of Applied Physics and Applied Mathematics, Columbia University, New York, NY, USA, [3]Department of Earth and Environmental Sciences, Columbia University, New York, NY, USA, [4]Lamont-Doherty Earth Observatory, Columbia University, Palisades, NY, USA

Key Points:

- We find a large summertime increase in the frequency, interannual variability, and persistence of a regime with a Greenland anticyclone
- Hindcasts and forecasts from SEAS5, an initialized seasonal model, are randomly sampled to generate a 10,000-member ensemble from 1981 to 2024
- The model is unable to capture the observed trends in regime frequency and variability owing to a lack of trends in persistence

Supporting Information:

Supporting Information may be found in the online version of this article.

Correspondence to:

S. H. Lee,
shl21@st-andrews.ac.uk

Citation:

Lee, S. H., & Polvani, L. M. (2026). Increasing frequency and persistence of the summertime Greenland High regime not captured by a seasonal prediction model very large ensemble. *Geophysical Research Letters*, *53*, e2025GL119421. https://doi.org/10.1029/2025GL119421

Received 16 SEP 2025
Accepted 6 DEC 2025

Abstract Weather regimes are widely used in weather prediction, but less often to study climate variability and change. Here, we use a year-round North American regime classification to identify summertime circulation trends from 1981 to 2024. We find large increases in the frequency, persistence and interannual variability of the Greenland High (GH) regime, similar to Greenland blocking. A simple Markov model shows that the observed increased GH frequency and variability can arise from increased persistence. We then show that a 10,000-member ensemble using SEAS5 seasonal model data fails to capture the observed trend in GH frequency because persistence trends are too weak. This occurs despite SEAS5 producing summers with more GH days and individual regimes more persistent than observed, so the issue is not simply an overall lack of persistence. Hence, the missing trends must arise from fundamental model deficiencies which develop on subseasonal timescales and are not rectified by initialization.

Plain Language Summary The weather across a region can be categorized into several patterns which occur repeatedly. Climate change—either natural or human-caused—can lead to some patterns occurring more often or lasting longer. We look at trends in daily weather patterns across North America during summer over the last 44 years. One pattern, named the 'Greenland High' (GH) because it features unusually high pressure near Greenland, has recently occurred more often and lasted longer. The number of days on which it occurs has also varied more from one summer to the next. We statistically show that an increase in the persistence can explain these trends. We then look at 10,000 different possible evolutions of the past 44 years using data from an operational seasonal forecasting model. While the model can produce extremely long-lasting GH patterns or summers with lots of GH days, it cannot produce the observed trends because it cannot produce the increasing trend in persistence. Therefore, similar problems previously reported in climate models are also present in seasonal models. This is a problem because it reduces our ability to forecast summer weather and to understand and predict long-term changes in weather patterns.

1. Introduction

"Weather regimes" are recurrent, persistent and quasi-stationary atmospheric circulation patterns which dominate mid-latitude low-frequency, super-synoptic variability (e.g., Michelangeli et al., 1995). Typically defined through clustering, regimes have been extensively studied over the North Atlantic–European sector (e.g., Cassou, 2008; Cassou et al., 2004; Cortesi et al., 2021; Grams et al., 2017; Michelangeli et al., 1995; Vautard, 1990) and more recently over North America (Lee et al., 2023; Nabizadeh et al., 2022; Robertson et al., 2020; Straus et al., 2007; Vigaud et al., 2018). Moving beyond the traditional focus on individual seasons, year-round weather regimes have been defined for the North Atlantic–European sector (Grams et al., 2017) and North America (Lee et al., 2023). Evidence from dynamical systems theory suggests that these regimes have a physical basis, representing persistent atmospheric states with low dimensionality (Hochman et al., 2021; Lee & Messori, 2024). Regimes have been widely used to understand large-scale subseasonal prediction (e.g., Büeler et al., 2021; Osman et al., 2023; Pérez-Carrasquilla & Molina, 2025), but have been relatively underutilized in analysis of observed and projected climate variability and change. This is particularly true of changes to regimes in seasons other than winter: although several recent studies have analyzed historical and projected changes in winter regimes over the Atlantic and Pacific (Dorrington, Strommen, & Fabiano, 2022; Dorrington, Strommen, Fabiano, &

Molteni, 2022; Fabiano et al., 2021), a regime-based view of historical changes in the summertime circulation over North America is lacking.

Motivating such an analysis are the large regional summertime circulation trends that have been observed in recent decades (reviewed by Shaw, Arias, et al., 2024). Notably, many summers in the 21st century—particularly since 2007—have seen an unusual dominance of Greenland blocking (e.g., Beckmann et al., 2025; Hanna et al., 2016; McLeod & Mote, 2016; J. R. Preece et al., 2023). This pattern consists of an anomalous mid-tropospheric anticyclone near Greenland, and is associated with the negative phase of the summer North Atlantic Oscillation (SNAO; Folland et al., 2009) and an equatorward-shifted Atlantic jet stream. A pattern similar to Greenland blocking appears as the "Greenland High" regime in the year-round North American regime classification of Lee et al. (2023); they reported a large increase in its summertime frequency over 1979–2022, noting it was the largest trend among the four regimes in any season.

Weather patterns comprising an anticyclone over Greenland during the melt season can exert a significant direct influence on the ice sheet (Hanna et al., 2014; J. Preece et al., 2022) and Arctic sea ice (Ding et al., 2017). This is in addition to the wider temperature and precipitation anomaly footprint from the circulation pattern across Europe and North America (e.g., Folland et al., 2009; Hanna, Hall, et al., 2018; Simonson et al., 2022). It is therefore vital that climate models accurately represent observed trends and variability in Greenland blocking and related patterns. However, the recent increase in summertime Greenland blocking is not captured by historical simulations from models contributing to the Coupled Model Intercomparison Project phase 5 (CMIP5) (Hanna, Fettweis, & Hall, 2018) or phase 6 (CMIP6) (Delhasse et al., 2021; Maddison et al., 2024). Atmosphere-only and anthropogenic aerosol-only experiments better represent past variability, but with much weaker amplitude than observed (Maddison et al., 2024). Furthermore, across CMIP5 and CMIP6, the majority of models project a *decrease* in summertime Greenland blocking (i.e., a more positive SNAO) in response to increased CO_2 (Davini & d'Andrea, 2020; Mitevski et al., 2025). Hence, the observed trend is both absent from historical climate model simulations, *and* opposite in sign to the expected response under increased greenhouse gas forcing.

Not yet explored is whether the summertime circulation trends over Greenland are captured by the *initialized* models used for seasonal prediction: this is a key goal of the present study. Seasonal model hindcasts are an underappreciated and underutilized resource for understanding the climate system. They can be leveraged to generate very large ensembles of potential climate trends (e.g., Thomas et al., 2025) or so-called "unseen" extremes (Thompson et al., 2017) without additional expense, because the data are produced routinely by operational prediction centers for model validation and calibration. Most seasonal models are similar to those used in CMIP, and their evaluations thus provides insight into the development of biases and trend errors in their uninitialized counterparts (Beverley et al., 2024; L'Heureux et al., 2022; Mayer et al., 2025).

Using the year-round North American weather regime classification of Lee et al. (2023), we here provide a detailed assessment of trends in the frequency of the summertime Greenland High weather regime over the last four decades. The regimes perspective connects local circulation trends over Greenland to the dominant continent-scale circulation patterns, while allowing simultaneous quantification of trends across all regimes and a straightforward analysis of large-scale circulation persistence. We then assess whether a very large 10,000-member ensemble constructed from a current-generation initialized, coupled seasonal prediction model can capture the regime trends.

2. Data and Methods

We base our study on ERA5 (Hersbach et al., 2020), the fifth generation reanalysis from the European Centre for Medium-Range Weather Forecasts (ECMWF), obtained once-daily at 0000 UTC on a 1.0° latitude–longitude grid from 1 January 1981 to 31 December 2024 (44 years). To investigate the regime trends within an initialized model, we take data from the 1 May initialization of SEAS5 (Johnson et al., 2019), the fifth generation ECMWF seasonal prediction system, over 1981–2024. The model output is obtained at the same temporal and horizontal resolution as the ERA5 data. SEAS5 is based upon Cy43r1 of the ECMWF Integrated Forecasting System (IFS), a more recent version of the IFS than Cy36r4 which underpins the CMIP6 EC-Earth3 model (Döscher et al., 2022). SEAS5 has a horizontal resolution of T319 and 91 vertical levels, and comprises 25-member hindcasts from 1981 to 2016 and 51-member operational forecasts from 2017 to 2024. Specifically, we use SEAS5 because of its large hindcast size (number of years × number of members) relative to other seasonal models, and the continuity

between hindcasts and operational forecasts. We use the first 25 members of the 51-member forecasts so as to have the same ensemble size for each initialization date (similar to Kolstad et al., 2022). Note that the hindcasts were initialized from ERA-Interim reanalysis (Dee et al., 2011) while the real-time forecasts were initialized from operational ECMWF analyses, but we find no evidence of discontinuities for the purposes of this study. SEAS5 includes time-varying greenhouse gas radiative forcing, which follows CMIP5 historical greenhouse gases from 1981 to 2005 and the CMIP5 RCP2.6 (also known as RCP3-PD) scenario thereafter. For further details, we refer the reader to Johnson et al. (2019).

North American weather regimes are calculated in ERA5 using a slightly modified version of the year-round method outlined in Lee et al. (2023). 500 hPa geopotential height (Z500) anomalies are first computed by subtracting the daily 1981–2024 climatology, which is smoothed with a 60-day centered running mean. The small difference from the 1979–2022 period in Lee et al. (2023) has negligible effect; the regimes are highly reproducible for different periods. To emphasize variability beyond synoptic timescales, we apply a 5-day centered running mean to the anomalies. This differs from the 10-day Fourier filter used in Lee et al. (2023), but we adopt it here as it is easier to apply to discontinuous forecast model output, while yielding the same regime attribution on 90% of days. We then de-trend the data by subtracting the trend in the cosine latitude-weighted area-average Z500 anomalies for each calendar day, smoothed with a 60-day running mean. This allows us to remove the mean-state thermal expansion of the Z500 surface while retaining circulation trends, and allows for seasonality in the trend which was not included by Lee et al. (2023); however, the impact of a seasonally-varying trend is minimal, with the same regime attribution on 96% of days if a fixed trend is used (and 95% of days if no de-trending is performed). Then, the seasonal cycle in the variance of the field is removed by dividing the daily anomalies by the 60-day smoothed cosine-latitude weighted domain-average grid-point standard deviation of the anomalies for each calendar day.

An empirical orthogonal function (EOF) decomposition of these normalized Z500 anomalies is then performed (with a square-root cosine-latitude weighting), and the leading 12 principal components (PCs) are retained (explaining 81% of the variance). k-means clustering is then performed on the 12 PCs with $k = 4$, and data points are assigned to clusters based on minimum Euclidean distance. Finally, days which are closer to climatology (i.e., all PCs equal to zero) than their assigned centroid are reassigned as "No Regime."

The resultant four regimes and their mean summertime (1 June–31 August) occurrence frequencies are Pacific Trough (PT; 20 days), Pacific Ridge (PR; 19 days), Alaskan Ridge (AKR; 15 days), and Greenland High (GH; 20 days). The remaining days are classified as No Regime (18 days). The average summertime Z500 anomalies for each regime are shown in Figure S1 in Supporting Information S1. For further information, we refer the reader to Lee et al. (2023).

In SEAS5, assuming each ensemble member represents a possible evolution of the atmosphere each summer, we create a 10,000 member ensemble (as in Thomas et al., 2025). We first choose a random member from each year to construct a synthetic 44-year time series. The data are then processed identically to the ERA5 description above: initially, we use May–September data to allow for the 60-day smoothing windows, before truncating to June–August. In order to work with a consistent set of weather regimes, we use the EOFs and regime centroids calculated from ERA5: we project the SEAS5 data onto the ERA5 EOFs to obtain pseudo-PCs, which are then assigned to regimes based on the minimum Euclidean distance to the ERA5 centroids. This process is then repeated 10,000 times—where each 44-year set of ensemble members is unique.

Statistical significance of linear trends is tested by bootstrap resampling with replacement 10,000 times. Two-sided p-values are obtained from the bootstrapped distribution as twice the probability of the sample statistic having the opposite sign. For trends computed on running mean time series, the resampling procedure is adjusted to account for autocorrelation by ensuring sampled data points are separated by the running mean window.

3. Observed Summertime Regime Trends

We begin by reporting the trends in the summertime frequency of the regimes over 1981–2024 according to ERA5, focusing on the Greenland High regime (Figure 1d). We find a significant increase in the frequency of the GH regime (+3.5 days decade^{-1}, $p = 0.04$), similar to the 1979–2022 trend reported in Lee et al. (2023). The summertime frequency of the GH regime is highly correlated with the summer NAO ($r = -0.84$) (e.g., Dunstone et al., 2023) and the Greenland Blocking Index (GBI) ($r = 0.88$ for GBI1 and $r = 0.84$ for GBI2 (Hanna

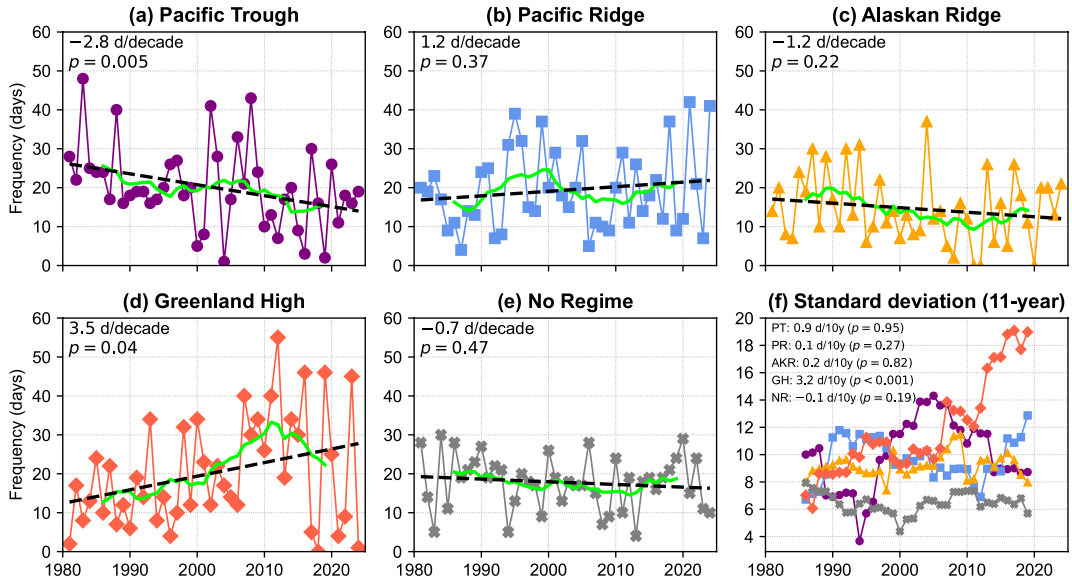

Figure 1. Summertime (June–August) frequency of the (a) Pacific Trough regime, (b) Pacific Ridge regime, (c) Alaskan Ridge regime, (d) Greenland High regime and (e) No Regime for 1981–2024 according to ERA5. Black dashed lines denote the linear trend. Solid green lines denote an 11-year centered moving average. (f) Standard deviation of the time series shown in (a–e), computed in 11-year centered periods. Linear trends and *p*-values are given in the top left of each panel.

et al., 2016; Hanna, Fettweis, & Hall, 2018)) (Figure S2 in Supporting Information S1). This confirms the ability of the year-round North American regime classification to identify similar summertime circulation patterns, and that such patterns are among the dominant ones across the North American continent. The exceptionally high frequency of the GH regime during the summers of 2012 (55 days), 2016 (46 days), 2019 (46 days) and 2023 (45 days) exceeded the frequency of a single regime in any summer except for the 48 days of PT in 1983 (Figure 1a). Both 2012 and 2019 saw extreme Greenland melt seasons (Hanna et al., 2014; Tedesco & Fettweis, 2020), while 2023 saw unusual warmth over high-latitude North America consistent with the GH regime, contributing to an extreme wildfire season (Jain et al., 2024). The occurrence of an exceptionally GH-dominated summer in 2023 (exceeding any year prior to 2012) suggests a continuation of the increased likelihood of the GH regime beyond the peak in the decadal frequency in the early 2010s. Although we focus on the 1981–2024 period here for comparison with SEAS5, the recent increased GH frequency remains exceptional when considering the full ERA5 data set back to 1940 (Figure S3d in Supporting Information S1), consistent with GBI-based analyses (Hanna et al., 2016; Maddison et al., 2024).

In Figure 1f one can also see a clear increase in the interannual variability of GH frequency (+3.2 days decade^{-1}, $p < 0.001$), computed here as the 11-year rolling standard deviation, resulting in an approximate doubling of the variability across the 44 years. Juxtaposed with the extremely GH-dominated summers of 2016, 2019, and 2023 are the summers of 2017, 2018, 2021, 2022, and 2024, which saw fewer than 10 GH days (zero in the case of 2018, which saw an extremely positive SNAO (Drouard et al., 2019)). The GH frequency during these five summers would have been below-average even at the start of the period. Hence, while summers with an extremely high GH frequency have become more likely, summers with a relatively low GH frequency have continued to occur.

As for the other regimes, we find no significant trends in the frequency of the PR regime (+1.2 days decade^{-1}, $p = 0.37$), the AKR regime (−1.2 days decade^{-1}, $p = 0.22$), or the No Regime (−0.7 days decade^{-1}, $p = 0.47$), but we note a significant decrease in the frequency of the PT regime (−2.8 days decade^{-1}, $p = 0.005$). However, when extending the regimes back to 1940, the reduced occurrence of the PT regime in recent years is not exceptional (Figure S3a in Supporting Information S1). In fact, the downward trend appears at least partly due to the shorter 1981–2024 period starting during unusually high PT frequency. The PT regime also does not show a significant change in interannual variability, and so we focus on the GH regime hereafter.

Increased regime frequency and increased interannual variability can arise due to increased persistence once a transition to the regime has occurred. Figure 2 provides three different diagnostics which all show that the GH

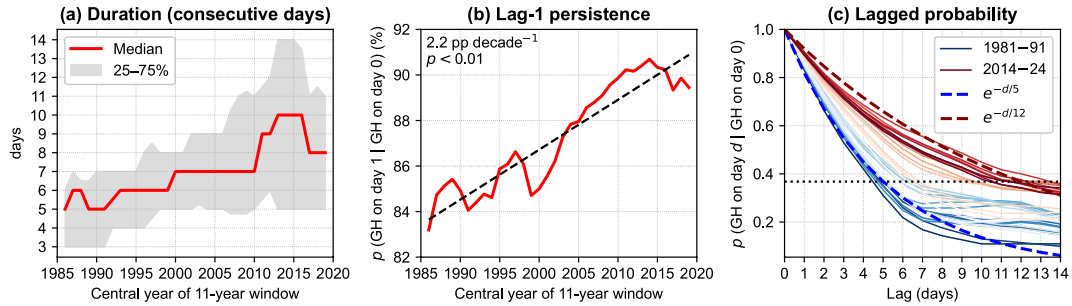

Figure 2. For 11-year centered overlapping windows: (a) time series of GH regime duration (consecutive days with the same regime). Red line denotes the median with shading from the 25th–75th percentiles. (b) Probability, in %, of the GH regime persisting into the next day (solid red line), with linear trend (black dashed line). (c) Lagged probability of the GH regime given the GH regime on day 0, where the line color denotes the 11-year time period (blues = older, reds = more recent). Blue and red dashed lines show exponential decay curves with e-folding timescales of 5 and 12 days respectively. Horizontal dotted line denotes $1/e$.

regime has become more persistent. The median regime duration, defined here as consecutive days with the same regime attribution and computed in 11-year overlapping periods, has increased from 5 to 6 days in the 1980s/1990s to 8–10 days in the 2010s/2020s, at a rate of approximately 1 day decade^{-1} (Figure 2a). Similarly, the probability of the GH regime persisting into the next day—the lag-1 persistence probability—has increased at a rate of 2.2 pp decade^{-1} ($p < 0.01$), from 84% in the 1980s to around 90% in the most recent decade (Figure 2b). The e-folding time of the regime, defined here as the number of days before a least-squares exponential fit to the function $p(GH$ on day $d|GH$ on day 0) decays below $1/e$, has approximately doubled from 5 days to 10–12 days (Figure 2c). On five occasions in five separate summers, the GH regime persisted for more than 3 weeks (27 days in 2019, 26 days in 2009, 25 days in 2023, 25 days in 1993, and 22 days in 2011), indicating potential windows of subseasonal predictability should models be able to accurately simulate the processes involved.

4. Markov Model

To further demonstrate the role of persistence in driving the frequency trend, we use a first-order two-state Markov model with either fixed or time varying persistence probabilities. The model is run 10,000 times each for the two variants. The time-varying lag-1 persistence probabilities, $\hat{p}(\mathrm{GH}_{t+1}|\mathrm{GH}_t)$, are taken as the linear fit to the lag-1 persistence probabilities computed over 11-year centered overlapping periods (cf. Figure 2b):

$$\hat{p}_{vary}(\mathrm{GH}_{t+1}|\mathrm{GH}_t) = 2.18 \times 10^{-3} y - 3.499, \quad y \in [1986, 2019] \tag{1}$$

The fixed persistence probabilities are computed using the full 44-year data set, yielding:

$$\hat{p}_{fix}(\mathrm{GH}_{t+1}|\mathrm{GH}_t) = 0.878 \tag{2}$$

In this simple model, we assume the probability of transitioning into the GH regime from the "Other" state is a constant and use the value computed across 1981–2024:

$$\hat{p}(\mathrm{GH}_{t+1}|\mathrm{Other}_t) = 0.035 \tag{3}$$

Under fixed persistence probabilities, the median frequency trend is zero and the probability of obtaining a trend greater than the ERA5 trend is 1.6%. With linearly-varying persistence probabilities, the probability of obtaining a trend greater than the ERA5 trend is 27.5% and thus statistically indistinguishable from the observed trend (Figure S4a in Supporting Information S1). Hence, the observed trend in regime frequency can be statistically attributed to increased regime persistence.

We also assess the probability of obtaining a trend in the standard deviation of the season-total frequency (computed over 11-year centered overlapping periods). Under fixed persistence probabilities, the probability of obtaining a trend greater than that in ERA5 is 1.3%. When the time-varying persistence probabilities are used, this

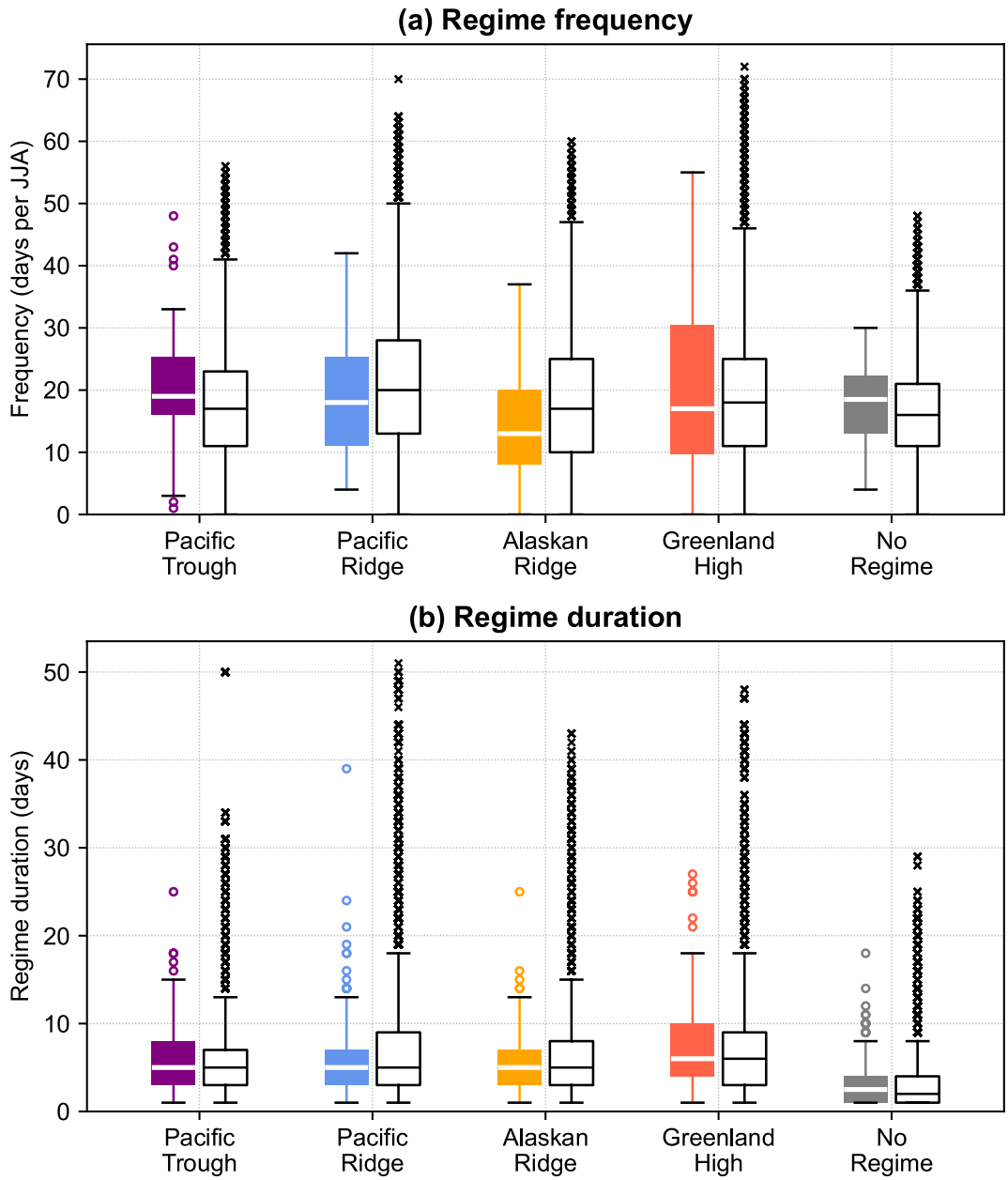

Figure 3. Boxplots of summertime (a) regime frequency and (b) regime duration (consecutive days with the same regime assignment) for ERA5 (left-hand colored boxes) and SEAS5 (right-hand unfilled boxes) 1981–2024. Whiskers extend to 1.5 × the interquartile range or to the extrema, with outliers marked as open circles (ERA5) and crosses (SEAS5).

increases to 6.7%, and is thus marginally captured by the simple Markov model (Figure S4b in Supporting Information S1). This is because, for a 92-day summer, solely increasing regime persistence raises the likelihood of summers with a high regime frequency more than it reduces the likelihood of summers with a low regime frequency, similar to the observed GH behavior (cf. Figure 1d).

5. Summertime Regimes in SEAS5

We now turn to examining the summertime regimes in the initialized SEAS5 model. Before assessing trends in the regimes, we first assess whether the model can simulate regimes of a similar frequency and duration to those in ERA5. Considering the full distribution of regime durations and seasonal frequencies over 1981–2024, the median summer regime frequencies are similar (±2 days) for all but the AKR regime (Figure 3a), which is slightly

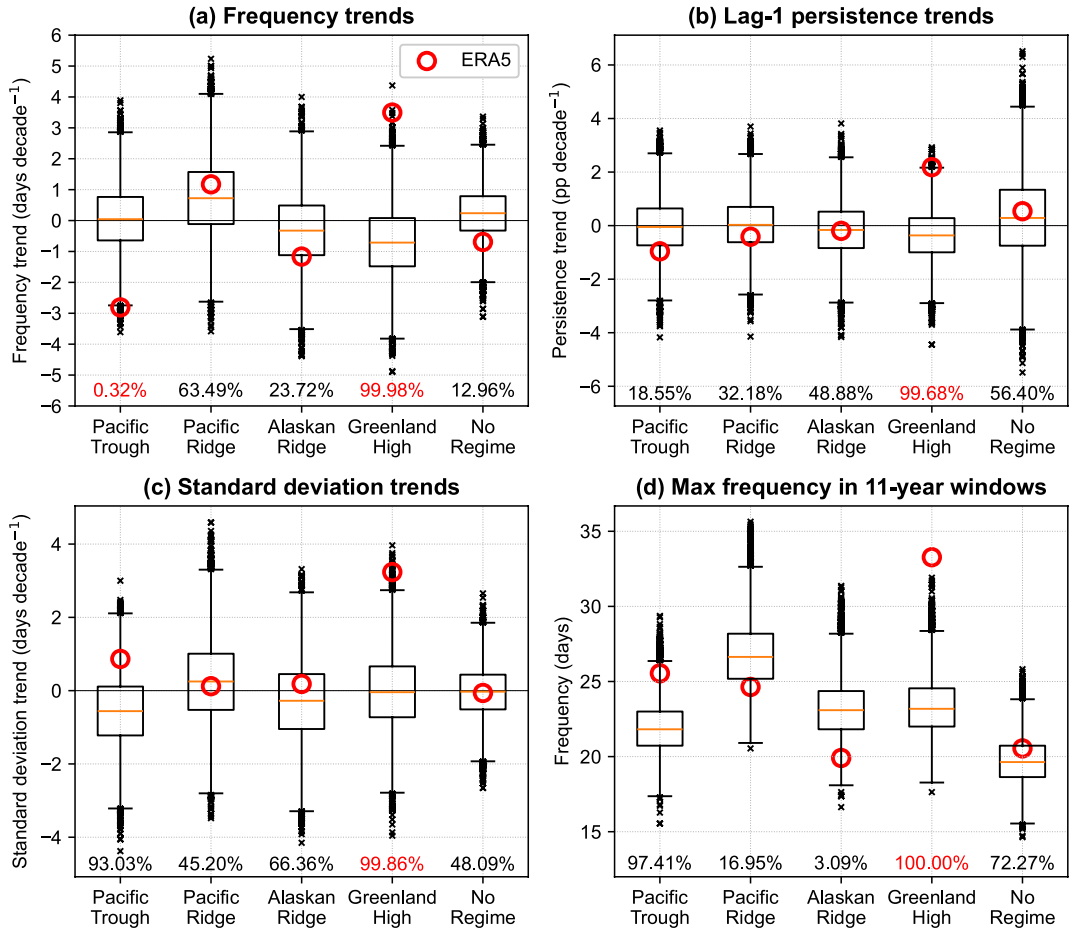

Figure 4. Boxplots of trends in (a) regime frequency, (b) lag-1 regime persistence and (c) seasonal frequency standard deviation in SEAS5. In (b) and (c), the standard deviation is computed over 11-year centered running windows prior to trend calculation. (d) Boxplots of the maximum 11-year running mean frequency. Red open circles denote the ERA5 trends. Percentages denote the fraction of SEAS5 members less than the ERA5 value; those outside 2.5%–97.5% are shown in red.

more likely in SEAS5 (17 days) than ERA5 (13 days). Reassuringly, our 10,000-member SEAS5 ensemble includes summers with a greater total regime frequency than those seen in ERA5 for all four regimes and No Regime, with an overall maximum of 72 days of GH in 2006 (78% of the season and 17 days longer than the observed maximum in 2012). Considering all ensemble members and all years, the probability of a summer more dominated by a single regime than in ERA5 is smallest for GH (0.1%) compared to 0.4% for PT, 3.5% for No Regime, 4.2% for PR and 4.9% for AKR.

Across all regime instances, the median regime durations (Figure 3b) are nearly identical between ERA5 and SEAS5 (5 days for PT, PR and AKR; 6 days for GH and 2 days for No Regime). However, for all regimes the SEAS5 ensemble features far more persistent events than those so far observed. These include 48 consecutive GH days (3 weeks longer than the most persistent GH regime in ERA5 and 52% of the season) and an overall maximum of 51 consecutive PR days. Hence, SEAS5 is able to simulate more extreme GH regime summers than those observed in terms of both regime dominance and overall regime persistence. Nevertheless, relative to other regimes, we note that the observed GH frequency extremes (Figure 3a) fall at the top end of the model distribution.

While SEAS5 can produce extreme GH events, the observed increasing trends in GH regime frequency, persistence and standard deviation are vanishingly unlikely within our 10,000-member ensemble. The probability of obtaining a trend greater than or equal to that in ERA5 is only 0.02% for GH frequency (Figure 4a), 0.32% for GH persistence (Figure 4b), and 0.14% for GH standard deviation (Figure 4c). For all three metrics, the GH trends are by far the most extreme across the five classes; while the decline in PT frequency is only exceeded by 0.32% of

SEAS5 ensemble members, it is not accompanied by a similarly extreme rank in persistence or standard deviation. In fact, SEAS5 shows a small median *declining* trend in both the frequency (-0.7 days decade^{-1}) and persistence (-0.4 pp decade^{-1}) of the GH regime consistent with the expected forced response to increased CO_2; the frequency trend is equal and opposite to the PR trend, while the persistence trend is the largest among the five classes. Additionally, SEAS5 fails to capture the observed decadal peak in GH frequency (Figure 4d): the peak 11-year running mean GH frequency of 33.3 days (2006–2016) lies beyond the maximum in the SEAS5 ensemble (31.9 days) and remains above the 95th percentile through the end of the record (Figure S5 in Supporting Information S1), even for our very large 10,000-member ensemble.

Finally, we note that across the ensemble, trends in GH persistence and trends in frequency are moderately correlated ($r = 0.44$, $p < 0.001$; Figure S6a in Supporting Information S1) as are trends in GH persistence and standard deviation ($r = 0.40$, $p < 0.001$; Figure S6b in Supporting Information S1). With the additional insight gained from the reanalysis-based Markov model, this relationship indicates that the inability of the model to produce the observed frequency and standard deviation trends can be attributed to insufficient trends in persistence.

6. Summary and Discussion

The discrepancy between the observed increase in summertime Greenland blocking and its absence from historical simulations using *uninitialized* climate models is well-known but poorly understood (Shaw, Arias, et al., 2024). Here, using the year-round, daily weather regime classification for North America introduced by Lee et al. (2023), we have found that such a discrepancy is present even in a 10,000-member ensemble of the current-generation *initialized* seasonal prediction model SEAS5. We demonstrated that the increasing persistence of the GH regime has played a central role in the increasing GH frequency and interannual variability. We then showed that SEAS5 fails to reproduce the frequency and variability trends not due to a general lack of GH regime persistence, but because its GH persistence *trends* are too weak.

The inability of SEAS5 to represent the observed GH trends provides one more example of a model bias that is not rectified by initialization, indicating that it must develop on relatively short (i.e., subseasonal) timescales (L'Heureux et al., 2022; Beverley et al., 2024; Lee & Polvani, 2024; Mayer et al., 2025). We therefore encourage a more unified approach, analyzing both initialized/seasonal models and uninitialized/climate models to help solve persistent modeling challenges across timescales (Randall & Emanuel, 2024; Shaw, Arblaster, et al., 2024). While we have only considered a single model, our results are consistent with the low probability of obtaining the observed SNAO trend in a similarly large ensemble of Met Office DePreSys3 hindcasts over 1981–2022 (Thomas et al., 2025).

Increased persistence implies increased predictability, particularly on medium-range to subseasonal timescales given the lifespan of extremely persistent regimes. This is deserving of further investigation. One limiting factor is the relatively short hindcast periods (~20-year) typically used, but trends in persistence should be considered when assessing model skill and skill differences between model versions/hindcast periods. Further, Strommen and Palmer (2019) proposed that insufficient regime persistence can lead to the signal-to-noise "paradox" seen in seasonal predictions of the NAO; whether trends in persistence play a role is an open question.

Several avenues exist for determining why the persistence of the GH regime has increased, and why this is missing from SEAS5. Synoptic-scale potential vorticity analyses (Hauser et al., 2024) could provide process-based insight. On larger scales, Arctic amplification (AA) has been linked to weaker summertime westerlies and more persistent circulation patterns (reviewed by Coumou et al., 2018). CMIP6 models also under-represent observed AA during summer (Rantanen et al., 2022). It does not immediately follow that this should affect the GH regime specifically, but may be related to eddy feedbacks (e.g., Barnes & Hartmann, 2010) since both the GH regime and AA weaken the meridional Z500 gradient.

Finally, while the persistence of the summertime GH regime has significantly increased, we do not argue that the regime will *continue* to become more persistent (some physical limits must eventually apply). If the CMIP models are to be believed, which one hesitates to do as they fail to capture the observed trends, the GH regime trends would actually *reverse* in the coming decades as a consequence of increasing greenhouse gases. The key question —whether or not the increased GH frequency that has occurred is a result of anthropogenic forcing—remains difficult to answer.

Conflict of Interest

The authors declare no conflicts of interest relevant to this study.

Data Availability Statement

The ERA5 data are openly available via the Copernicus Climate Data Store (CDS) at https://doi.org/10.24381/cds.bd0915c6 (Copernicus Climate Change Service, Climate Data Store, 2023). The SEAS5 data are openly available via the CDS at https://doi.org/10.24381/cds.50ed0a73 with the system identifier 51 (Copernicus Climate Change Service, Climate Data Store, 2018). The processed regime data supporting this study are available online at https://doi.org/10.5281/zenodo.17937714 (Lee & Polvani, 2025).

Acknowledgments
Data processing was performed using the University of St Andrews high performance computing facility, *Hypatia*. LMP is funded, in part, from award 2335762 from the US National Science Foundation to Columbia University. We thank Kristian Strommen and an anonymous reviewer for their very helpful comments.

References

Barnes, E. A., & Hartmann, D. L. (2010). Dynamical feedbacks and the persistence of the NAO. *Journal of the Atmospheric Sciences*, *67*(3), 851–865. https://doi.org/10.1175/2009JAS3193.1

Beckmann, J., Di Capua, G., & Davini, P. (2025). Summer Greenland Blocking in observations and in SEAS5. 1 seasonal forecasts: Robust trend or natural variability? *EGUsphere*, *2025*, 1–34. https://doi.org/10.5194/egusphere-2024-3998

Beverley, J. D., Newman, M., & Hoell, A. (2024). Climate model trend errors are evident in seasonal forecasts at short leads. *npj Climate and Atmospheric Science*, *7*(1), 285. https://doi.org/10.1038/s41612-024-00832-w

Büeler, D., Ferranti, L., Magnusson, L., Quinting, J. F., & Grams, C. M. (2021). Year-round sub-seasonal forecast skill for Atlantic–European weather regimes. *Quarterly Journal of the Royal Meteorological Society*, *147*(741), 4283–4309. https://doi.org/10.1002/qj.4178

Cassou, C. (2008). Intraseasonal interaction between the Madden–Julian Oscillation and the North Atlantic Oscillation. *Nature*, *455*(7212), 523–527. https://doi.org/10.1038/nature07286

Cassou, C., Terray, L., Hurrell, J. W., & Deser, C. (2004). North Atlantic winter climate regimes: Spatial asymmetry, stationarity with time, and oceanic forcing. *Journal of Climate*, *17*(5), 1055–1068. https://doi.org/10.1175/1520-0442(2004)017<1055:NAWCRS>2.0.CO;2

Copernicus Climate Change Service, Climate Data Store. (2018). Seasonal forecast subdaily data on pressure levels [Dataset]. *Copernicus Climate Change Service (C3S) Climate Data Store (CDS)*. https://doi.org/10.24381/cds.50ed0a73

Copernicus Climate Change Service, Climate Data Store. (2023). ERA5 hourly data on pressure levels from 1940 to present [Dataset]. *Copernicus Climate Change Service (C3S) Climate Data Store (CDS)*. https://doi.org/10.24381/cds.bd0915c6

Cortesi, N., Torralba, V., Lledó, L., Manrique-Suñén, A., Gonzalez-Reviriego, N., Soret, A., & Doblas-Reyes, F. J. (2021). Yearly evolution of Euro-Atlantic weather regimes and of their sub-seasonal predictability. *Climate Dynamics*, *56*(11–12), 3933–3964. https://doi.org/10.1007/s00382-021-05679-y

Coumou, D., Di Capua, G., Vavrus, S., Wang, L., & Wang, S. (2018). The influence of Arctic amplification on mid-latitude summer circulation. *Nature Communications*, *9*(1), 2959. https://doi.org/10.1038/s41467-018-05256-8

Davini, P., & d'Andrea, F. (2020). From CMIP3 to CMIP6: Northern Hemisphere atmospheric blocking simulation in present and future climate. *Journal of Climate*, *33*(23), 10021–10038. https://doi.org/10.1175/JCLI-D-19-0862.1

Dee, D. P., Uppala, S. M., Simmons, A. J., Berrisford, P., Poli, P., Kobayashi, S., et al. (2011). The ERA-Interim reanalysis: Configuration and performance of the data assimilation system. *Quarterly Journal of the Royal Meteorological Society*, *137*(656), 553–597. https://doi.org/10.1002/qj.828

Delhasse, A., Hanna, E., Kittel, C., & Fettweis, X. (2021). Brief communication: CMIP6 does not suggest any atmospheric blocking increase in summer over Greenland by 2100. *International Journal of Climatology*, *41*(4), 2589–2596. https://doi.org/10.1002/joc.6977

Ding, Q., Schweiger, A., L'Heureux, M., Battisti, D. S., Po-Chedley, S., Johnson, N. C., et al. (2017). Influence of high-latitude atmospheric circulation changes on summertime Arctic Sea Ice. *Nature Climate Change*, *7*(4), 289–295. https://doi.org/10.1038/nclimate3241

Dorrington, J., Strommen, K., & Fabiano, F. (2022). Quantifying climate model representation of the wintertime Euro-Atlantic circulation using geopotential-jet regimes. *Weather and Climate Dynamics*, *3*(2), 505–533. https://doi.org/10.5194/wcd-3-505-2022

Dorrington, J., Strommen, K., Fabiano, F., & Molteni, F. (2022). CMIP6 models trend toward less persistent European blocking regimes in a warming climate. *Geophysical Research Letters*, *49*(24), e2022GL100811. https://doi.org/10.1029/2022GL100811

Döscher, R., Acosta, M., Alessandri, A., Anthoni, P., Arneth, A., Arsouze, T., et al. (2022). The EC-Earth3 Earth system model for the coupled model intercomparison project 6. *Geoscientific Model Development*, *15*(7), 2973–3020. https://doi.org/10.5194/gmd-15-2973-2022

Drouard, M., Kornhuber, K., & Woollings, T. (2019). Disentangling dynamic contributions to summer 2018 anomalous weather over Europe. *Geophysical Research Letters*, *46*(21), 12537–12546. https://doi.org/10.1029/2019GL084601

Dunstone, N., Smith, D. M., Hardiman, S. C., Hermanson, L., Ineson, S., Kay, G., et al. (2023). Skilful predictions of the summer North Atlantic Oscillation. *Communications Earth & Environment*, *4*(1), 409. https://doi.org/10.1038/s43247-023-01063-2

Fabiano, F., Meccia, V. L., Davini, P., Ghinassi, P., & Corti, S. (2021). A regime view of future atmospheric circulation changes in northern mid-latitudes. *Weather and Climate Dynamics*, *2*(1), 163–180. https://doi.org/10.5194/wcd-2-163-2021

Folland, C. K., Knight, J., Linderholm, H. W., Fereday, D., Ineson, S., & Hurrell, J. W. (2009). The summer North Atlantic Oscillation: Past, present, and future. *Journal of Climate*, *22*(5), 1082–1103. https://doi.org/10.1175/2008JCLI2459.1

Grams, C. M., Beerli, R., Pfenninger, S., Staffell, I., & Wernli, H. (2017). Balancing Europe's wind-power output through spatial deployment informed by weather regimes. *Nature Climate Change*, *7*(8), 557–562. https://doi.org/10.1038/nclimate3338

Hanna, E., Cropper, T. E., Hall, R. J., & Cappelen, J. (2016). Greenland Blocking Index 1851–2015: A regional climate change signal. *International Journal of Climatology*, *36*(15), 4847–4861. https://doi.org/10.1002/joc.4673

Hanna, E., Fettweis, X., & Hall, R. J. (2018). Brief communication: Recent changes in summer Greenland blocking captured by none of the CMIP5 models. *The Cryosphere*, *12*(10), 3287–3292. https://doi.org/10.5194/tc-12-3287-2018

Hanna, E., Fettweis, X., Mernild, S. H., Cappelen, J., Ribergaard, M. H., Shuman, C. A., et al. (2014). Atmospheric and oceanic climate forcing of the exceptional Greenland ice sheet surface melt in summer 2012. *International Journal of Climatology*, *34*(4), 1022–1037. https://doi.org/10.1002/joc.3743

Hanna, E., Hall, R. J., Cropper, T. E., Ballinger, T. J., Wake, L., Mote, T., & Cappelen, J. (2018). Greenland blocking index daily series 1851–2015: Analysis of changes in extremes and links with North Atlantic and UK climate variability and change. *International Journal of Climatology*, *38*(9), 3546–3564. https://doi.org/10.1002/joc.5516

Hauser, S., Teubler, F., Riemer, M., Knippertz, P., & Grams, C. M. (2024). Life cycle dynamics of Greenland blocking from a potential vorticity perspective. *Weather and Climate Dynamics*, *5*(2), 633–658. https://doi.org/10.5194/wcd-5-633-2024

Hersbach, H., Bell, B., Berrisford, P., Hirahara, S., Horányi, A., Muñoz-Sabater, J., et al. (2020). The ERA5 global reanalysis. *Quarterly Journal of the Royal Meteorological Society*, *146*(730), 1999–2049. https://doi.org/10.1002/qj.3803

Hochman, A., Messori, G., Quinting, J. F., Pinto, J. G., & Grams, C. M. (2021). Do Atlantic-European weather regimes physically exist? *Geophysical Research Letters*, *48*(20), e2021GL095574. https://doi.org/10.1029/2021GL095574

Jain, P., Barber, Q. E., Taylor, S. W., Whitman, E., Castellanos Acuna, D., Boulanger, Y., et al. (2024). Drivers and impacts of the record-breaking 2023 wildfire season in Canada. *Nature Communications*, *15*(1), 6764. https://doi.org/10.1038/s41467-024-51154-7

Johnson, S. J., Stockdale, T. N., Ferranti, L., Balmaseda, M. A., Molteni, F., Magnusson, L., et al. (2019). SEAS5: The new ECMWF seasonal forecast system. *Geoscientific Model Development*, *12*(3), 1087–1117. https://doi.org/10.5194/gmd-12-1087-2019

Kolstad, E. W., Lee, S. H., Butler, A. H., Domeisen, D. I., & Wulff, C. O. (2022). Diverse surface signatures of stratospheric polar vortex anomalies. *Journal of Geophysical Research: Atmospheres*, *127*(20), e2022JD037422. https://doi.org/10.1029/2022JD037422

Lee, S. H., & Messori, G. (2024). The dynamical footprint of year-round North American Weather Regimes. *Geophysical Research Letters*, *51*(2), e2023GL107161. https://doi.org/10.1029/2023GL107161

Lee, S. H., & Polvani, L. M. (2024). Large model biases in the Pacific Centre of the Northern Annular Mode due to exaggerated variability of the Aleutian Low. *Quarterly Journal of the Royal Meteorological Society*, *150*(764), 4478–4497. https://doi.org/10.1002/qj.4825

Lee, S. H., & Polvani, L. M. (2025). Data for "Increasing frequency and persistence of the summertime Greenland High regime not captured by a seasonal prediction model very large ensemble" [Dataset]. *Zenodo*. https://doi.org/10.5281/zenodo.17937714

Lee, S. H., Tippett, M. K., & Polvani, L. M. (2023). A new year-round weather regime classification for North America. *Journal of Climate*, *36*(20), 7091–7108. https://doi.org/10.1175/JCLI-D-23-0214.1

L'Heureux, M. L., Tippett, M. K., & Wang, W. (2022). Prediction challenges from errors in tropical Pacific Sea surface temperature trends. *Frontiers in Climate*, *4*, 837483. https://doi.org/10.3389/fclim.2022.837483

Maddison, J., Catto, J., Hanna, E., Luu, L., & Screen, J. (2024). Missing increase in summer Greenland blocking in climate models. *Geophysical Research Letters*, *51*(11), e2024GL108505. https://doi.org/10.1029/2024GL108505

Mayer, M., Balmaseda, M. A., Vitart, F., & Tietsche, S. (2025). Tropical Pacific trends in the ECMWF seasonal system and implications for predictions of the 2020–22 Triple-Dip La Niña. *Journal of Climate*, *38*(13), 2989–3003. https://doi.org/10.1175/JCLI-D-24-0467.1

McLeod, J. T., & Mote, T. L. (2016). Linking interannual variability in extreme Greenland blocking episodes to the recent increase in summer melting across the Greenland ice sheet. *International Journal of Climatology*, *36*(3), 1484–1499. https://doi.org/10.1002/joc.4440

Michelangeli, P.-A., Vautard, R., & Legras, B. (1995). Weather regimes: Recurrence and quasi stationarity. *Journal of the Atmospheric Sciences*, *52*(8), 1237–1256. https://doi.org/10.1175/1520-0469(1995)052<1237:WRRAQS>2.0.CO;2

Mitevski, I., Lee, S. H., Vecchi, G., Orbe, C., & Polvani, L. M. (2025). More positive and less variable North Atlantic Oscillation at high CO_2 forcing. *npj Climate and Atmospheric Science*, *8*(1), 171. https://doi.org/10.1038/s41612-025-01051-7

Nabizadeh, E., Lubis, S. W., & Hassanzadeh, P. (2022). The summertime Pacific-North American weather regimes and their predictability. *Geophysical Research Letters*, *49*(16), e2022GL099401. https://doi.org/10.1029/2022GL099401

Osman, M., Beerli, R., Büeler, D., & Grams, C. M. (2023). Multi-model assessment of sub-seasonal predictive skill for year-round Atlantic-European weather regimes. *Quarterly Journal of the Royal Meteorological Society*, *149*(755), 2386–2408. https://doi.org/10.1002/qj.4512

Pérez-Carrasquilla, J. S., & Molina, M. J. (2025). An Earth-system-oriented view of the S2S predictability of North American Weather Regimes. *Artificial Intelligence for the Earth Systems*, *4*(3), 1–25. https://doi.org/10.1175/AIES-D-24-0075.1

Preece, J. R., Wachowicz, L., Mote, T., Tedesco, M., & Fettweis, X. (2022). Summer Greenland blocking diversity and its impact on the surface mass balance of the Greenland ice sheet. *Journal of Geophysical Research: Atmospheres*, *127*(4), e2021JD035489. https://doi.org/10.1029/2021JD035489

Preece, J. R., Mote, T. L., Cohen, J., Wachowicz, L. J., Knox, J. A., Tedesco, M., & Kooperman, G. J. (2023). Summer atmospheric circulation over Greenland in response to Arctic amplification and diminished spring snow cover. *Nature Communications*, *14*(1), 3759. https://doi.org/10.1038/s41467-023-39466-6

Randall, D. A., & Emanuel, K. (2024). The weather–climate schism. *Bulletin of the American Meteorological Society*, *105*(1), E300–E305. https://doi.org/10.1175/BAMS-D-23-0124.1

Rantanen, M., Karpechko, A. Y., Lipponen, A., Nordling, K., Hyvärinen, O., Ruosteenoja, K., et al. (2022). The Arctic has warmed nearly four times faster than the globe since 1979. *Communications Earth & Environment*, *3*(1), 168. https://doi.org/10.1038/s43247-022-00498-3

Robertson, A. W., Vigaud, N., Yuan, J., & Tippett, M. K. (2020). Toward identifying subseasonal forecasts of opportunity using North American weather regimes. *Monthly Weather Review*, *148*(5), 1861–1875. https://doi.org/10.1175/MWR-D-19-0285.1

Shaw, T. A., Arblaster, J. M., Birner, T., Butler, A. H., Domeisen, D., Garfinkel, C. I., et al. (2024). Emerging climate change signals in atmospheric circulation. *AGU Advances*, *5*(6), e2024AV001297. https://doi.org/10.1029/2024AV001297

Shaw, T. A., Arias, P. A., Collins, M., Coumou, D., Diedhiou, A., Garfinkel, C. I., et al. (2024). Regional climate change: Consensus, discrepancies, and ways forward. *Frontiers in Climate*, *6*, 1391634. https://doi.org/10.3389/fclim.2024.1391634

Simonson, J. M., Birkel, S. D., Maasch, K. A., Mayewski, P. A., Lyon, B., & Carleton, A. M. (2022). Association between recent US northeast precipitation trends and Greenland blocking. *International Journal of Climatology*, *42*(11), 5682–5693. https://doi.org/10.1002/joc.7555

Straus, D. M., Corti, S., & Molteni, F. (2007). Circulation regimes: Chaotic variability versus SST-forced predictability. *Journal of Climate*, *20*(10), 2251–2272. https://doi.org/10.1175/JCLI4070.1

Strommen, K., & Palmer, T. N. (2019). Signal and noise in regime systems: A hypothesis on the predictability of the North Atlantic Oscillation. *Quarterly Journal of the Royal Meteorological Society*, *145*(718), 147–163. https://doi.org/10.1002/qj.3414

Tedesco, M., & Fettweis, X. (2020). Unprecedented atmospheric conditions (1948–2019) drive the 2019 exceptional melting season over the Greenland ice sheet. *The Cryosphere*, *14*(4), 1209–1223. https://doi.org/10.5194/tc-14-1209-2020

Thomas, R., Woollings, T., & Dunstone, N. (2025). The role of internal variability in seasonal hindcast trend errors. *Journal of Climate*, *1*(19), 5541–5553. https://doi.org/10.1175/JCLI-D-24-0367.1

Thompson, V., Dunstone, N. J., Scaife, A. A., Smith, D. M., Slingo, J. M., Brown, S., & Belcher, S. E. (2017). High risk of unprecedented UK rainfall in the current climate. *Nature Communications*, *8*(1), 107. https://doi.org/10.1038/s41467-017-00275-3

Vautard, R. (1990). Multiple weather regimes over the North Atlantic: Analysis of precursors and successors. *Monthly Weather Review*, *118*(10), 2056–2081. https://doi.org/10.1175/1520-0493(1990)118<2056:MWROTN>2.0.CO;2

Vigaud, N., Robertson, A. W., & Tippett, M. K. (2018). Predictability of recurrent weather regimes over North America during winter from submonthly reforecasts. *Monthly Weather Review*, *146*(8), 2559–2577. https://doi.org/10.1175/MWR-D-18-0058.1